Estimation of vehicle sideslip angle and tire-road friction coefficient based on magnetometer with GPS

Article *in* International Journal of Automotive Technology · June 2016

DOI: 10.1007/s12239-016-0044-7

CITATIONS
29

READS
653

3 authors, including:

Shengbo Eben Li
Tsinghua University
213 PUBLICATIONS **5,542** CITATIONS

SEE PROFILE

International Journal of Automotive Technology, Vol. 17, No. 3, pp. 427–435 (2016)
DOI 10.1007/s12239–015–0044–7

pISSN 1229–9138/ eISSN 1976–3832

ESTIMATION OF VEHICLE SIDESLIP ANGLE AND TIRE-ROAD FRICTION COEFFICIENT BASED ON MAGNETOMETER WITH GPS

J.-H. YOON[1)], S. EBEN LI[2)] and C. AHN[3)*]

[1)]System and Control Design, TRW Automotive, Livonia, Michigan 48150, USA
[2)]State Key Lab of Automotive Safety and Energy, Tsinghua University, Beijing 100048, China
[3)]School of Mechanical Engineering, Pusan National University, Busan 46241, Korea

(Received 7 January 2015; Revised 10 November 2015; Accepted 29 November 2015)

ABSTRACT–This paper presents a method that estimates the vehicle sideslip angle and a tire-road friction coefficient by combining measurements of a magnetometer, a global positioning system (GPS), and an inertial measurement unit (IMU). The estimation algorithm is based on a cascade structure consisting of a sensor fusing framework based on Kalman filters. Several signal conditioning techniques are used to mitigate issues related to different signal characteristics, such as latency and disturbances. The estimated sideslip angle information and a brush tire model are fused in a Kalman filter framework to estimate the tire-road friction coefficient. The performance and practical feasibility of the proposed approach were evaluated through several tests.

KEY WORDS : GPS, Kalman filter, Magnetometer, Sideslip angle, Tire-road friction coefficient

1. INTRODUCTION

The dynamic control of ground vehicles during severe maneuvering requires accurate information on vehicle states and road conditions. In particular, the sideslip angle and the tire-road friction coefficient are the most critical information for design and control of vehicle control systems. However, these two pieces of information are not directly measurable in passenger vehicles due to technical and cost constraints. Consequently, many researchers have proposed methodologies to estimate these two pieces of information.

To estimate the sideslip angle, vehicle dynamics and tire models have been used (Farrelly and Wellstead, 1996; Best *et al.*, 2000; Stephant *et al.*, 2004; Grip *et al.*, 2008). Dynamic model-based methods have shown the ability to estimate sideslip angles. However, these methods require accurate vehicle parameter information such as cornering stiffness, vehicle mass and moment of inertia, and they work only for small sideslip angles. To avoid the issues in plant parameter uncertainties, IMU integration-based methods have been proposed (Farrelly and Wellstead, 1996; Imsland *et al.*, 2006). This type of method does not require accurate vehicle parameters and works well even for large sideslip angles. However, unknown biases in the sensor measurements can significantly degrade the estimation accuracy. To increase the immunity to the sensor biases, a dual-antenna GPS receiver has been included in the estimation framework (Ryu and Gerdes, 2004a, 2004b). The velocity information from GPS does not have biases; therefore, this method significantly improves the accuracy of estimation. However, it is too expensive to be used in production vehicles (Piyabongkarn *et al.*, 2009). Low cost GPS-based methods (Bevly, 2004; Yoon and Peng, 2010; Bevly *et al.*, 2002) have been proposed and demonstrated in terms of estimation capability.

The tire-road friction coefficient estimation methods can be classified by the types of sensors used. Camera-image based methods (Holzmann *et al.*, 2006; Yamada *et al.*, 2005; Sato *et al.*, 2007) have advantages that the friction coefficient can be detected for the road surface ahead of the vehicle and the estimation is independent of vehicle motions. However these methods are solely dependent on road conditions. Most of the friction coefficient estimation methods are based on vehicle and tire models. Wheel and tire model-based methods (Ito *et al.*, 1994; Liu and Peng, 1996; Gustafsson, 1998; Umeno *et al.*, 2002) are based only on wheel velocity sensors; however, they are quite vulnerable to high frequency disturbances. Because vehicle dynamics are much slower than the wheel dynamics, they are inherently robust to high frequency noises. Therefore many methods are based on vehicle dynamics with a tire model. These methods are usually based on the vehicle sideslip angle measured using external equipment, because the friction coefficient is highly coupled with the tire slip angle in the tire model. As described previously, the sideslip measurement is cost prohibitive. Therefore, practical estimation approaches (Ahn *et al.*, 2012, 2013;

*Corresponding author. e-mail: sunahn@pusan.ac.kr

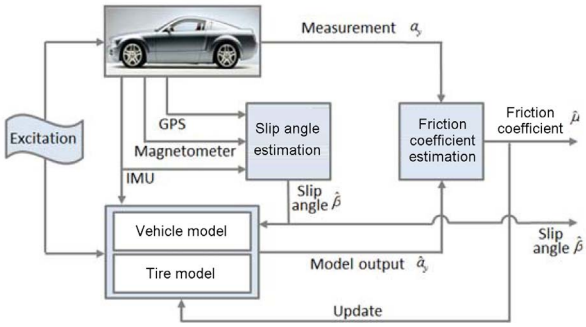

Figure 1. Estimation diagram.

Hsu and Gerdes, 2006) have been proposed to estimate the sideslip angle and the friction coefficient using the tire aligning moment with conventional IMU measurement. These methods showed the practical possibility of simultaneous estimation of the sideslip angle and the friction coefficient. However, the sideslip angle estimation is affected by the accuracy of the model.

This paper proposes a practical method to simultaneously estimate the vehicle sideslip angle and the tire-road friction coefficient for a wide range of vehicle motions. The proposed method combines measurements of the velocity from a single antenna GPS, local magnetic fields from a magnetometer and angular-velocity/ acceleration from an IMU. In addition, we introduce a method to reject large errors in magnetometer measurements that is integrated with a Kalman filter framework. We also present a method that addresses delays in low-cost GPS measurements. The overall estimation diagram is in Figure 1. The velocity signals from GPS, the angular signals from a magnetometer, and the acceleration and angular velocity signals from an IMU are fused in the Kalman filters to estimate the vehicle sideslip angles. For the friction coefficient estimation, the vehicle lateral acceleration (a_y) is measured and also predicted through the system models. Based on the measured and predicted values, a Kalman filter estimates the frictional coefficient.

The remainder of this paper is organized as follows. In Section 2, we describe the mathematical techniques used to integrate several sensor signals. In Section 3, we discuss extended Kalman filters for sideslip angle estimation. In Section 4, we describe the friction coefficient estimation based on an extended Kalman filter with the vehicle and tire models. Section 5 presents the results of experimental verification. Our conclusions are presented in Section 6.

2. MATHEMATICAL TECHNIQUES FOR ESTIMATION SYNTHESIS

The estimation is based on multiple sensors and corresponding systems are nonlinear, which naturally casts into the framework of the extended Kalman filter. Even though the Kalman filter provides an optimal estimation, the characteristics of sensor signals must be considered in the design of the estimator. One of the authors published papers on the disturbance rejection and time-delay (Yoon and Peng, 2010, 2014). We improved the disturbance rejection algorithm with a simple but equally effective methodology and applied the same time-delay handling technique to this case. In this section, we briefly describe the basic knowledge of the extended Kalman filter and signal conditioning techniques.

2.1. Extended Kalman Filter Framework

A Kalman filter provides the optimal state estimation for linear systems. For nonlinear systems, the Kalman filter can be applied to a linearized version of the system equations. This is called an extended Kalman filter. For the extended Kalman filter design, the transition and measurement models are expressed as follows;

$$\begin{aligned} x_{\mathrm{k}} &= f(x_{\mathrm{k-1}}, u_{\mathrm{k-1}}) + w_{\mathrm{k-1}}, \\ y_{\mathrm{k}} &= h(x_{\mathrm{k}}) + v_{\mathrm{k}}, \end{aligned} \tag{1}$$

where, x is a state vector, u is the input, y is measurement, k is the index for time steps, and w_{k} and v_{k} are the process and measurement noises, respectively, which are assumed to be zero mean Gaussian noises with covariance Q_{k} and R_{k}, respectively. The design synthesis of the extended Kalman filter is described as follows;

$$\begin{aligned} &\hat{x}_{\mathrm{k|k-1}} = f(\hat{x}_{\mathrm{k-1|k-1}}, u_{\mathrm{k-1}}), \\ &P_{\mathrm{k|k-1}} = F_{\mathrm{k-1}} P_{\mathrm{k-1|k-1}} {F^T}_{\mathrm{k-1}} + Q_{\mathrm{k-1}}, \\ &\tilde{y}_{\mathrm{k}} = y_{\mathrm{k}} - h(\hat{x}_{\mathrm{k|k-1}}), \\ &K_{\mathrm{k}} = P_{\mathrm{k|k-1}} {H^{\mathrm{T}}}_{\mathrm{k}} \left(H_{\mathrm{k}} P_{\mathrm{k|k-1}} {H^{\mathrm{T}}}_{\mathrm{k}} + R_{\mathrm{k}} \right)^{-1}, \\ &\hat{x}_{\mathrm{k|k}} = \hat{x}_{\mathrm{k|k-1}} + K_{\mathrm{k}} \tilde{y}_{\mathrm{k}}, \\ &P_{\mathrm{k|k}} = (I - K_{\mathrm{k}} H_{\mathrm{k}}) P_{\mathrm{k|k-1}}, \end{aligned} \tag{2}$$

where $F_{\mathrm{k-1}}$ and H_{k} are the Jacobian matrices of f and h, respectively, as follows;

$$F_{\mathrm{k-1}} = \left. \frac{\partial f}{\partial x} \right|_{\hat{\mathrm{x}}_{\mathrm{k-1|k-1}}, \mathrm{u}_{\mathrm{k-1}}}, \; H_{\mathrm{k-1}} = \left. \frac{\partial h}{\partial x} \right|_{\hat{\mathrm{x}}_{\mathrm{k-1|k-1}}}. \tag{3}$$

2.2. Disturbance Rejection

Because the Earth's magnetic field is weak, metal objects near the magnetometer can induce significant disturbances. The basis of magnetic disturbances detection is that the magnetic field norm deviates from a nominal value when disturbances exist. The disturbance rejection is designed using this basis with the concept of the Mahalanobis distance (Mahalanobis, 1936). The Mahalanobis distance characterizes the similarity of an arbitrary data set to another data set in a normalized distance. The Mahalanobis distance is scale-invariant and defined by the following equation;

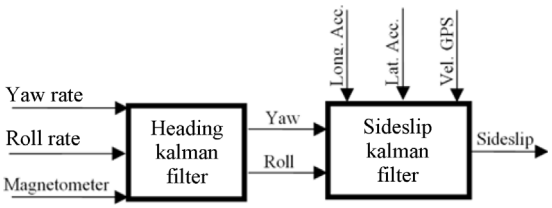

Figure 2. Schematic diagram of sideslip angle estimation.

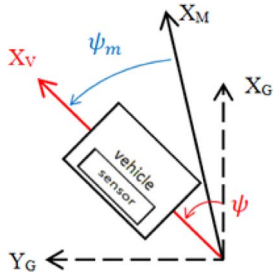

Figure 3. Top view of four coordinate frames.

$$d(\vec{x},\vec{y}) = \sqrt{(\vec{x}-\vec{y})^{\mathrm{T}} S^{-1} (\vec{x}-\vec{y})}. \tag{4}$$

where S is the covariance matrix. When a measurement update is available, the Kalman filter provides the covariance matrix.

When this distance is larger than a predetermined threshold, the measured signals are less reliable. The threshold is calculated from the chi-square cumulative distribution. For our case, H_k is replaced with a zero matrix when the Mahalanobis distance exceeds the threshold in order to reject the disturbances in the measurement update process.

2.3. Delay Handling

Velocity measurements using a low-cost GPS receiver are known to have a significant delay (Ryu and Gerdes, 2004b; Yoon and Peng, 2010). To address this issue, we used the idea of "measurement shifting" described by Larsen (Larsen *et al.*, 1998). The GPS delay must be known to apply the measurement shifting technique. When a vehicle accelerates (or decelerates) during straight driving, the delay in GPS velocity measurements can be observed by comparing it to the vehicle velocity calculated from the wheel speed sensors.

3. SIDESLIP ANGLE ESTIMATION

Figure 2 shows a schematic overview of two Kalman filters used to estimate the vehicle sideslip angles. The heading Kalman filter estimates the yaw and roll angles by processing angular rate signals and magnetic field measurements. Then, the vehicle sideslip is calculated through the sideslip Kalman filter by combining vehicle velocities measured by a single GPS receiver with vehicle accelerations from an IMU.

3.1. Coordinate Frames

Figure 3 shows four sets of coordinate frames used in this study. The symbol G represents the geographic Earth-fixed frame (G-frame). X_G and Y_G point to the geographic north and west. M is another Earth-fixed frame (M-frame) whose X-axis (X_M) points to magnetic north. The frame "v" is a moving frame on the vehicle (v-frame). Each frame is related to one another through yaw-pitch-roll angles.

$$\begin{bmatrix} m_x \\ m_y \\ m_z \end{bmatrix} = \begin{bmatrix} \cos\psi_m \cos\theta_m & \\ -\sin\psi_m \cos\phi_m + \cos\psi_m \sin\theta_m \sin\phi_m & \\ \sin\psi_m \sin\phi_m + \cos\psi_m \sin\theta_m \cos\phi_m & \end{bmatrix}$$
$$\begin{bmatrix} \sin\psi_m \cos\theta_m & -\sin\theta_m \\ \cos\psi_m \cos\phi_m + \sin\psi_m \sin\theta_m \sin\phi_m & \cos\theta_m \sin\phi_m \\ -\cos\psi_m \sin\phi_m + \sin\psi_m \sin\theta_m \cos\phi_m & \cos\theta_m \cos\phi_m \end{bmatrix} \begin{bmatrix} M_x \\ M_y \\ M_z \end{bmatrix}, \tag{5}$$

A magnetometer measures the Earth's magnetic field in the v-frame. Since the Earth's magnetic vector is the constant vector pointing to magnetic north in the M-frame, magnetometer measurements can be expressed by rotations of the magnetometer. By using the ZYX Euler angle definition, the kinematic equation is obtained as Equation (5), where $[m_x, m_y, m_z]^T$ is the Earth magnetic field measured in the v-frame, $[M_x, M_y, M_z]^T$ is the Earth magnetic field measured in the M-frame, and $[\psi_m, \theta_m, \phi_m]$ is a vector of yaw, pitch, and roll angles of the magnetometer with respect to the M-frame.

GPS velocity measurements are provided in the G-frame, so $(\psi+\psi_o, \theta+\theta_o, \phi+\phi_o) = (\psi_m, \theta_m, \phi_m)$ where (ψ, θ, ϕ) are the Euler angles representing the vehicle attitude in the G-frame. The subscript "o" represents constant offset values. These offsets are known values and determined by calibration.

3.2. Heading Angle Filter

At each data sampling, the magnetometer provides only one directional vector. However, to fully determine the attitude of a three-dimensional (3-D) object, at least two independent directional vectors are required. Therefore $[M_x, M_y, M_z]^T$ cannot be uniquely determined. With the assumption of a zero pitch angle, Equation (5) is converted into Equation (6) as follows;

$$g(\psi, \phi) = \begin{bmatrix} m_x \\ m_y \\ m_z \end{bmatrix} =$$
$$\begin{bmatrix} M_X \cos\psi_m - M_Z \theta_o \\ -M_X \sin\psi_m \cos\phi_m + M_X \theta_o \cos\psi_m \sin\phi_m + M_Z \sin\phi_m \\ M_X \sin\psi_m \cos\phi_m + M_X \theta_o \cos\psi_m \cos\phi_m + M_Z \cos\phi_m \end{bmatrix} \tag{6}$$

Because Equation (5) is nonlinear, the extended Kalman filter is used. For the time update equation, the transition dynamics of angular rates and angles are given by

$$\begin{bmatrix}\dot{\psi}\\ \dot{\phi}\end{bmatrix}=\begin{bmatrix}0 & 0\\ 0 & 0\end{bmatrix}\begin{bmatrix}\psi\\ \phi\end{bmatrix}+\begin{bmatrix}r_{\mathrm{m}}-b_{\mathrm{r}}\\ p_{\mathrm{m}}-b_{\mathrm{p}}\end{bmatrix}+noise, \tag{7}$$

where $[r_{\mathrm{m}}, p_{\mathrm{m}}]$ are the yaw rate and roll rate measurements and $[b_{\mathrm{r}}, b_{\mathrm{p}}]$ are the biases, which can be obtained through vehicle standstill tests.

3.3. Sideslip Angle Filter

In the International Organization for Standardization (ISO) coordinate system, the kinematics relating accelerations and velocities are given by

$$\begin{aligned} a_{\mathrm{x,m}} &= \dot{v}_{\mathrm{x}} + \dot{\psi} v_{\mathrm{y}} + b_{\mathrm{x}} + w_{\mathrm{x}},\\ a_{\mathrm{y,m}} &= \dot{v}_{\mathrm{y}} + \dot{\psi} v_{\mathrm{x}} + b_{\mathrm{y}} + g\sin\phi + w_{\mathrm{y}}, \end{aligned} \tag{8}$$

where $[a_{\mathrm{x,m}}, a_{\mathrm{y,m}}]$ are the longitudinal and lateral acceleration measurements, $[v_{\mathrm{x}}, v_{\mathrm{y}}]$ are the longitudinal and lateral velocities, $[b_{\mathrm{x}}, b_{\mathrm{y}}]$ are the biases in the accelerations, $g\sin\phi$ is the gravitational component by roll, and $[w_{\mathrm{x}}, w_{\mathrm{y}}]$ is the Gaussian white noise.

The yaw rate ($\dot{\psi}$) is obtained by subtracting the yaw rate bias from the yaw rate measurements, and Equation (8) is rearranged to form the time update equation as Equation (9). The accelerometer biases are augmented into the states to be estimated.

$$\begin{bmatrix}\dot{v}_{\mathrm{x}}\\ \dot{b}_{\mathrm{x}}\\ \dot{v}_{\mathrm{y}}\\ \dot{b}_{\mathrm{y}}\end{bmatrix}=\begin{bmatrix}0 & -1 & \dot{\psi} & 0\\ 0 & 0 & 0 & 0\\ -\dot{\psi} & 0 & 0 & -1\\ 0 & 0 & 0 & 0\end{bmatrix}\begin{bmatrix}v_{\mathrm{x}}\\ b_{\mathrm{x}}\\ v_{\mathrm{y}}\\ b_{\mathrm{y}}\end{bmatrix}+\begin{bmatrix}1 & 0\\ 0 & 0\\ 0 & 1\\ 0 & 0\end{bmatrix}\begin{bmatrix}a_{\mathrm{x,m}}\\ a_{\mathrm{y,m}}-g\sin\phi\end{bmatrix}+noise \tag{9}$$

A single antenna GPS can provide the vehicle velocity in the G-frame. The vehicle yaw and roll angles are known from the heading Kalman filter, and thus, vehicle velocity measurement in the G-frame can be converted into longitudinal, lateral and vertical velocities in the v-frame as follows;

$$\begin{bmatrix}v_{\mathrm{x}}^{\mathrm{GPS}}\\ v_{\mathrm{y}}^{\mathrm{GPS}}\\ v_{\mathrm{z}}^{\mathrm{GPS}}\end{bmatrix}=\begin{bmatrix}\cos\psi & \sin\psi & 0\\ -\cos\phi\sin\psi & \cos\phi\cos\psi & \sin\phi\\ \sin\phi\sin\psi & -\sin\phi\cos\psi & \cos\phi\end{bmatrix}\begin{bmatrix}V_{\mathrm{N}}^{\mathrm{GPS}}\\ V_{\mathrm{W}}^{\mathrm{GPS}}\\ V_{\mathrm{U}}^{\mathrm{GPS}}\end{bmatrix} \tag{10}$$

where $[V_{\mathrm{N}}^{\mathrm{GPS}}\ V_{\mathrm{W}}^{\mathrm{GPS}}\ V_{\mathrm{U}}^{\mathrm{GPS}}]$ are the velocities in the G-frame measured by GPS, $[v_{\mathrm{x}}^{\mathrm{GPS}}\ v_{\mathrm{y}}^{\mathrm{GPS}}\ v_{\mathrm{z}}^{\mathrm{GPS}}]$ are the velocities in the v-frame measured by GPS. The measurement update equations are

$$\begin{bmatrix}v_{\mathrm{x}}^{\mathrm{GPS}}\\ v_{\mathrm{y}}^{\mathrm{GPS}}\end{bmatrix}=\begin{bmatrix}1 & 0 & 0 & 0\\ 0 & 0 & 1 & 0\end{bmatrix}\begin{bmatrix}v_{\mathrm{x}}\\ b_{\mathrm{x}}\\ v_{\mathrm{y}}\\ b_{\mathrm{y}}\end{bmatrix}+noise \tag{11}$$

Once estimations of longitudinal and lateral velocities are obtained, the sideslip angle is given by

$$\hat{\beta}=\tan^{-1}\left(\hat{v}_{\mathrm{x}}/\hat{v}_{\mathrm{y}}\right), \tag{12}$$

where $\hat{\beta}$, $\hat{v}_{\mathrm{x}}$, and $\hat{v}_{\mathrm{y}}$ are estimations of the sideslip angle, longitudinal velocity, and sideslip angle by the sideslip Kalman filter, respectively.

4. FRICTION COEFFICIENT ESTIMATION

4.1. Vehicle Planar Model

The effects of the tire-road friction coefficient, the tire slip angle, and tire lateral force generation are highly coupled. A tire characterizes the relationship between the variables, and the tire lateral forces drive the vehicle lateral motions. Because the effects of the sideslip angle and the friction coefficient are measured through the vehicle lateral acceleration, the vehicle body dynamics characterize the relationship between the lateral acceleration and the two variables. Therefore, a vehicle model and a tire model are important elements in friction coefficient estimation.

The bicycle model represents the vehicle lateral dynamics as shown in Figure 4 and the lateral force on the vehicle is expressed as;

$$ma_{\mathrm{y}}=2f_{\mathrm{yf}}\cos\delta+2f_{\mathrm{yr}}, \tag{13}$$

where a_{y} is the vehicle lateral acceleration; m is the vehicle mass; f_{yf} and f_{yr} are the lateral force at the front and rear tires, respectively; and δ is the front tire's road steer angle. Taking the small angle approximation, we can write tire slip angles α_{f} and α_{r} that for the front and rear tires respectively,

$$\begin{aligned}\alpha_{\mathrm{f}} &= \delta-(\beta+ar/v_{\mathrm{x}}),\\ \alpha_{\mathrm{r}} &= -(\beta-br/v_{\mathrm{x}}),\end{aligned} \tag{14}$$

where a and b are the distances from vehicle center of gravity to the front and rear axles, respectively; v_{x} is the vehicle longitudinal speed; and r is the yaw rate.

The lateral force generated between the tires and the road is a nonlinear function of the tire slip angle α and friction coefficient μ. The brush tire model would be a good choice because it needs fewer parameters to evaluate the tire/road forces than other tire models (Dugoff *et al.*, 1969; Canudas de Wit and Tsiotras, 1999; Pacejka, 2005), which is a great benefit for control and estimation

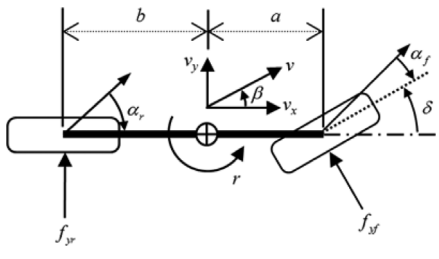

Figure 4. Vehicle lateral dynamics model.

Table 1. Sensor specifications.

	Manufacturer/Model name	Sampling rate	Noise level (1σ)	Note
Magnetometer	Xsens/MTi	120 Hz	0.5 mG	
IMU	Delphi/–	166 Hz	0.02 m/s^2 0.08 deg/s	Production ESC unit
Low cost GPS	–	5 Hz		Emulated
Reference signal measurement	Oxford/RT2500	100 Hz	0.05 m/s 0.02 deg/s	

purposes. The lateral tire force generation model is given by

$$\begin{aligned} &if\ \alpha \le \alpha_{sl} \\ &\quad f_y = 3\mu F_z \theta_y \sigma_y \left\{ 1 - \left|\theta_y \sigma_y\right| + \tfrac{1}{3}\left(\theta_y \sigma_y\right)^2 \right\}, \\ &else \\ &\quad f_y = \mu F_z \,\mathrm{sgn}(\alpha), \end{aligned} \tag{15}$$

where $\alpha_{sl} = \tan^{-1}(1/\theta_y)$, $\theta_y = 2c_p l^2/(3\mu F_z)$, $\sigma_y = \tan(\alpha)$, l is one-half of the tire contact patch length, α is the tire slip angle, μ is the tire-road frictional coefficient, F_z is the tire normal force, and c_p is the stiffness coefficient of the tire tread in unit length. In the brush tire model, only two parameters (l and c_p) characterize the tire properties.

4.2. Estimation Algorithm for the Friction Coefficient

The friction coefficient is estimated using the extended Kalman filter. For the filter design, the transition and measurement models are expressed as follows;

$$\begin{aligned} &f(\mu_{k-1}) = \mu_{k-1}, \\ &h(\mu_k) = a_y(\mu_k) = \frac{1}{m}\left(2f_y(\alpha_f, \mu_k)\cos\delta + 2f_y(\alpha_r, \mu_k)\right), \end{aligned} \tag{16}$$

where μ is the friction coefficient. We note that the tire slip angles α_f and α_r are functions of the sideslip angle β, which that is known. The estimator design for the friction coefficient follows the extended Kalman filter design in Equations (2) and (3).

5. VALIDATION RESULTS

Experimental verification was conducted in two steps. The first step was tire model identification through on-track tests and the second step was algorithm verification on a test track and public roads. On the test track, the test vehicle was driven with standard test maneuvers, such as a double lane change and slalom. On public roads, the test vehicle was driven to emulate daily driving patterns.

The test vehicle was a GM Silverado pickup truck equipped with several sensors that are described in Table 1. The RT2500 (Oxford Technical Solutions, UK) provided the reference signal, and measured the sideslip angle, at a 100 Hz sampling rate. To emulate the velocity signals of a low-cost GPS receiver, an artificial 400 ms delay was injected into the signals and the signal was down-sampled at 5 Hz.

Figure 5. Experimental setup on a test vehicle.

5.1. Tire Model Identification

The parameters for vehicle models, such as mass and length, were obtained from the manufacturer's vehicle specifications. However, the tire parameters, l and c_p, were identified from the pure lateral tests. The parameters were identified by minimizing the error between the model and the measured lateral accelerations. Figure 6 shows the model validation with test results on a packed snow surface.

5.2. On-track Experiments

Experimental verification was conducted on a test track on two types of surfaces: packed snow and ice. The packed snow surface on the test track had a friction coefficient in the range of 0.2 to 0.3. The ice surface had a friction coefficient from 0.1 to 0.2.

To represent the estimation results, two types of

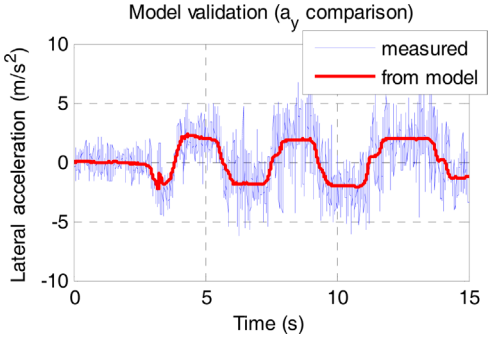

Figure 6. Tire model validation.

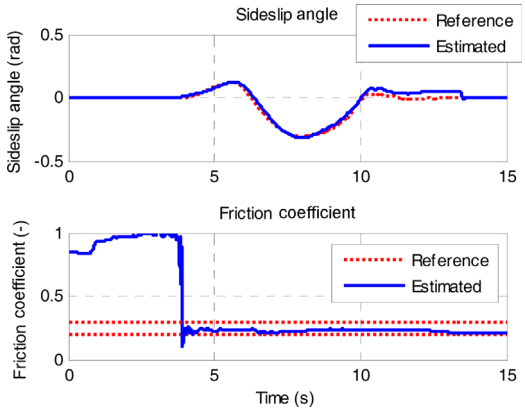

Figure 7. Estimation results of a double lane change test on a packed snow surface.

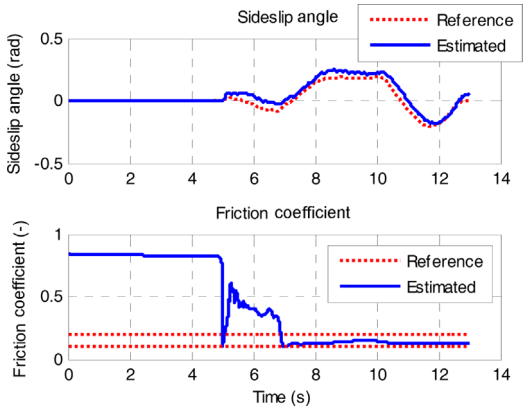

Figure 9. Estimation results of a double lane change test on an ice surface.

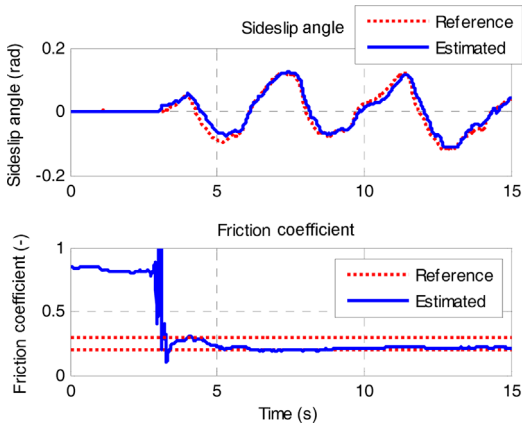

Figure 8. Estimation results of a slalom test on a packed snow surface.

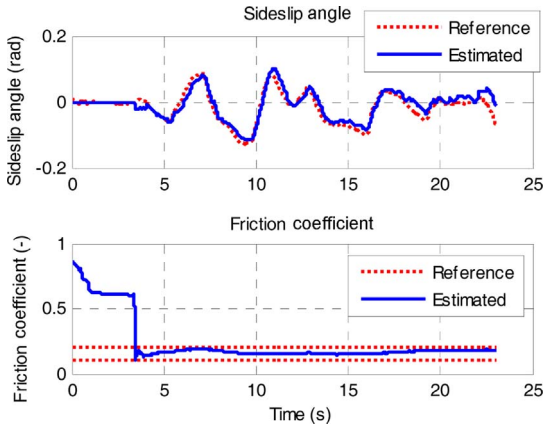

Figure 10. Estimation results of a slalom test on an ice surface.

maneuvers including a double lane change and slalom on packed snow and ice surfaces, are shown in Figures 7 to 10. The red dotted lines in the sideslip angle plots are reference signals from the RT2500, and the blue lines are estimations using the proposed method. The red dotted lines in the friction coefficient plots represent the range of the friction coefficient. The sideslip estimation remained close to the reference signal and the friction coefficient converged to the reference value. Data from multiple tests on several types of vehicle maneuvers were collected. The root mean squares error of the sideslip angle from 70 collected runs was 1.3°.

The friction coefficient estimation works well when there are sufficient excitations, which are large yaw rate signals or large sideslip angles, because if the lateral acceleration is very small, then the measurement update term in the Kalman filter is less effective. When excitations are not sufficient, the estimated friction coefficient is not reliable, which is noticeably shown during the period from 5 to 7 seconds shown in Figure 9. The amount of excitations required for a reliable estimation is dependent on the accuracies of the tire model and sideslip angle estimation (Ahn, 2011).

5.3. Public Road Tests

The test places for public road experiments were neighborhood areas in Kinross, Michigan, USA. The tests were performed on February, 2012. Figure 11 shows a map of the area and two vehicle trajectories. Most of the roads were covered with snow. There were more natural disturbances than in the test track environment. Magnetic disturbance came from passing vehicles, houses, and utility poles with electric transformers. The road surfaces were not leveled as the test track, where as we assumed that road pitch angles are sufficiently small to be negligible. Several cornering maneuvers were tried to create considerable lateral excitations on the snow-covered roads.

Figures 12 and 13 show the estimation results of two public road experiments. The estimated sideslip angles remained close to the reference signal. Again, the estimated friction coefficient did not converged to the true value until there were sufficient lateral excitations. Overall, the

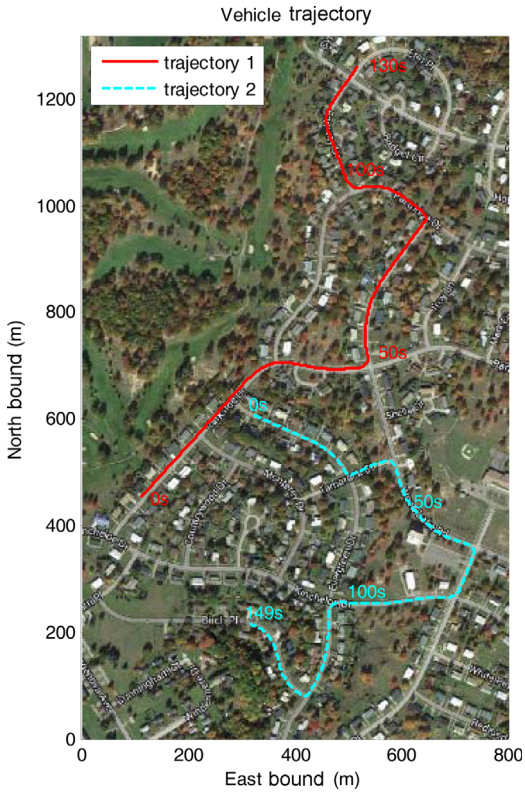

Figure 11. Top view of the area used for tests (Kinross, Michigan, USA). The actual tests were performed on snowy public roads in the winter.

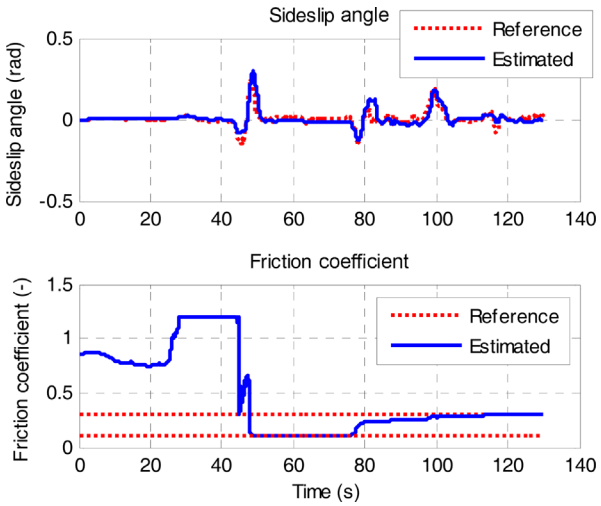

Figure 12. Estimation results on public roads (trajectory 1). The vehicle velocity was about 30 km/h.

sideslip angle estimation tracked the reference signal successfully. However, the root mean squre error of slideslip angles from all collected runs was 2.45 degrees, which is worse than the on-track test results. This accuracy degradation occurred due non-negligible pitch angles in the public road environment.

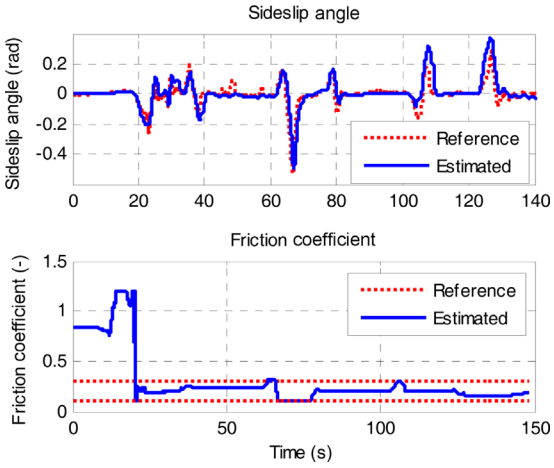

Figure 13. Estimation results on public roads (trajectory 2). The vehicle velocity was about 30 km/h.

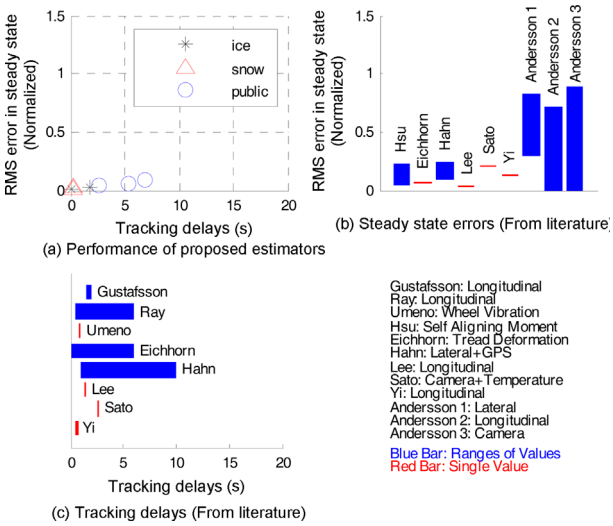

Figure 14. Performance comparison: (a) Performance of proposed estimators; (b) Steady-state errors (from literature); (c) Tracking delays (from literature).

Figure 14 shows performance of the esimator in the tests. The normalized steady state estimation errors of friction coefficient are within 0.0 ~ 0.2 and the delays are within 1 ~ 7 seconds, depending on excitation conditions. Figures 14 (b) and (c) show the steady state error and tracking delays obtained from literature (Gustafsson, 1997; Ray, 1997; Eichhorn and Roth, 1992; Hahn *et al.*, 2002; Lee *et al.*, 2004; Hsu *et al.*, 2006; Hsu and Gerdes, 2006; Sato *et al.*, 2007; Umeno *et al.*, 2002; Yi *et al.*, 1999; Andersson *et al.*, 2007), whose results may not be directly comparable to the estimator developed in this study because the surface conditions, tires, vehicles, and excitation conditions are all different. However, the proposed observer performs similar to or better than the algorithms found in the literature.

6. CONCLUSION

This paper presented a cost effective estimation method for the vehicle sideslip angle and the friction coefficient. The required sensors are a single antenna GPS, an IMU, and a magnetometer, which are already available in the market at low prices. The usefulness of magnetometers for ground vehicle applications has been highly questioned due to their susceptibility to large errors. However, this paper shows the feasibility of using a magnetometer for ground vehicle applications. The sideslip angle is estimated through serial Kalman filters and the friction coefficient is estimated based on vehicle lateral dynamics and the brush tire model. The proposed algorithm works across a wide range of side slips, which has been challenging to the existing algorithms. In the proposed method, we assumed that no longitudinal tire force and no pitch angle exist. The existence of longitudinal tire forces affects the lateral and forward directional behavior of the tires and the pitch angles affect the solution of Equation (5). These should be considered for implementation into a vehicle. We leave these topics for future study.

REFERENCES

Ahn, C. (2011). *Robust Estimation of Road Friction Coefficient for Vehicle Active Safety Systems.* Ph. D. Dissertation. The University of Michigan. Ann Arbor, USA.

Ahn, C., Peng, H. and Tseng, H. E. (2012). Robust estimation of road friction coefficient using lateral and longitudinal vehicle dynamics. *Vehicle System Dynamics* **50**, **6**, 961–985.

Ahn, C., Peng, H. and Tseng, H. E. (2013). Robust estimation of road frictional coefficient. *IEEE Trans. Control Systems Technology* **21**, **1**, 1–13.

Andersson, M., Bruzelius, F., Casselgren, J., Gäfvert, M., Hjort, M., Hultén, J., Håbring, F., Klomp, M., Olsson, G., Sjödahl, M., Svendenius, J., Woxneryd, S. and Wälivaara, B. (2007). Road Friction Estimation. Intelligent Vehicle Safety Systems. 2004:17750.

Best, M. C., Gordon, T. J. and Dixon, P. J. (2000). An extended adaptive Kalman filter for real-time state estimation of vehicle handling dynamics. *Vehicle System Dynamics* **34**, **1**, 57–75.

Bevly, D. M. (2004). Global positioning system (GPS): A low-cost velocity sensor for correcting inertial sensor errors on ground vehicles. *J. Dynamic Systems, Measurement, and Control* **126**, **2**, 255–264.

Bevly, D. M., Gerdes, J. C. and Wilson, C. (2002). The use of GPS based velocity measurements for measurement of sideslip and wheel slip. *Vehicle System Dynamics* **38**, **2**, 127–147.

Canudas De Wit, C. and Tsiotras, P. (1999). Dynamic tire friction models for vehicle traction control. *IEEE Int. Conf. Decision and Control*, Phoenix, Arizona, USA, 3746–3751.

Dugoff, H., Fancher, P. S. and Segel, L. (1969). Tire Performance Characteristics Affecting Vehicle Response to Steering and Braking Control Inputs. Highway Safety Research Institute. PB187-667.

Eichhorn, U. and Roth, J. (1992). Prediction and monitoring of tyre/road friction. *FISITA*, London, UK, 67–74.

Farrelly, J. and Wellstead, P. (1996). Estimation of vehicle lateral velocity. *IEEE Int. Conf. Control Applications*, Dearborn, MI, USA, 552–557.

Grip, H. a. F., Imsland, L., Johansen, T. A., Fossen, T. I., Kalkkuhl, J. C. and Suissa, A. (2008). Nonlinear vehicle side-slip estimation with friction adaptation. *Automatica* **44**, **3**, 611–622.

Gustafsson, F. (1997). Slip-based tire-road friction estimation. *Automatica* **33**, **6**, 1087–1099.

Gustafsson, F. (1998). Monitoring tire-road friction using the wheel slip. *IEEE Control Systems Magazine* **18**, **4**, 42–49.

Hahn, J.-O., Rajamani, R. and Alexander, L. (2002). GPS-based real-time identification of tire-road friction coefficient. *IEEE Trans. Control Systems Technology* **10**, **3**, 331–343.

Holzmann, F., Bellino, M., Siegwart, R. and Bubb, H. (2006). Predictive estimation of the road-tire friction coefficient. *IEEE Int. Conf. Control Applications*, Munich, Germany, 885–890.

Hsu, Y.-H. J. and Gerdes, J. C. (2006). A feel for the road: A method to estimate tire parameters using steering torque. *Int. Symp. Advanced Vehicle Control*, Taipei, Taiwan, 835–840.

Hsu, Y.-H. J., Laws, S., Gadda, C. D. and Gerdes, J. C. (2006). A method to estimate the friction coefficient and tire slip angle using steering torque. *Int. Mechanical Engineering Congress and Exposition*, Chicago, IL, USA, 515–524

Imsland, L., Johansen, T. A., Fossen, T. I., Fjær Grip, H., Kalkkuhl, J. C. and Suissa, A. (2006). Vehicle velocity estimation using nonlinear observers. *Automatica* **42**, **12**, 2091–2103.

Ito, M., Yoshioka, K. and Saji, T. (1994). Estimation of road surface conditions using wheel speed behavior. *Int. Symp. Advanced Vehicle Control*, Tsukuba, Japan, 533–538.

Larsen, T. D., Andersen, N. A., Ravn, O. and Poulsen, N. K. (1998). Incorporation of time delayed measurements in a discrete-time Kalman filter. *Conf. Decision and Control*, **4**, 3972–3977.

Lee, C., Hedrick, K. and Yi, K. (2004). Real time slip based estimation of maximum tire road friction coefficient. *IEEE/ASME Trans. Mechatronics* **9**, **2**, 454–458.

Liu, C.-S. and Peng, H. (1996). Road friction coefficient estimation for vehicle path prediction. *Vehicle System Dynamics* **25**, **1**, 413–425.

Mahalanobis, P. C. (1936). On the generalized distance in statistics. *Proc. National Institute of Sciences (Calcutta)*

2, **1**, 49–55.

Pacejka, H. B. (2005). *Tyre and Vehicle Dynamics.* Elsevier. Oxford, UK.

Piyabongkarn, D., Rajamani, R., Grogg, J. A. and Lew, J. Y. (2009). Development and experimental evaluation of a slip angle estimator for vehicle stability control. *IEEE Trans. Control Systems Technology* **17**, **1**, 78–88.

Ray, L. R. (1997). Nonlinear tire force estimation and road friction identification: simulation and experiments. *Automatica* **33**, **10**, 1819–1833.

Ryu, J. and Gerdes, J. C. (2004a). Estimation of vehicle roll and road bank angle. *American Control Conf.*, Boston, MA, USA, 2110–2115.

Ryu, J. and Gerdes, J. C. (2004b). Integrating inertial sensors with global positioning system (GPS) for vehicle dynamics control. *J. Dynamic Systems, Measurement, and Control* **126**, **2**, 243–254.

Sato, Y., Kobay, A. D., Kageyama, I., Watanabe, K., Kuriyagawa, Y. and Kuriyagawa, Y. (2007). Study on recognition method for road friction condition. *JSAE Trans.* **38**, **2**, 51–56.

Stephant, J., Charara, A. and Meizel, D. (2004). Virtual sensor: Application to vehicle sideslip angle and transversal forces. *IEEE Trans. Industrial Electronics* **51**, **2**, 278–289.

Umeno, T., Ono, E., Asano, K., Ito, S., Tanaka, A., Yasui, Y. and Sawada, M. (2002). Estimation of tire-road friction using tire vibration model. *SAE World Cong.*, Detroit, Michigan, USA.

Yamada, M., Ueda, K., Horiba, I., Tsugawa, S. and Yamamoto, S. (2005). Road surface condition detection technique based on image taken by camera attached to vehicle rearview mirror. *Review of Automotive Engineering* **26**, **2**, 163–168.

Yi, K., Hedrick, K. and Lee, S.-C. (1999). Estimation of tire-road friction using observer based identifiers. *Vehicle System Dynamics* **31**, **4**, 233–261.

Yoon, J.-H. and Peng, H. (2010). Vehicle sideslip angle estimation using two single-antenna GPS receivers. *Dynamic Systems and Control Conf.*, Boston, MA, USA, 863–870.

Yoon, J.-H. and Peng, H. (2014). Robust vehicle sideslip angle estimation through a disturbance rejection filter that integrates a magnetometer with GPS. *IEEE Trans. Intelligent Transportation Systems* **15**, **1**, 191–204.